

## Dynamic 3D Print of the Breathing Function

Duc Duong  
 Computational Physiology Lab  
 Univ. of Houston  
 Houston, TX  
 chiduc0880@yahoo.com

Dvijesh Shastri  
 Computer Science & Eng. Tech.  
 Univ. of Houston, Downtown  
 Houston, TX  
 shastrid@uhd.edu

Ioannis Pavlidis  
 Computational Physiology Lab  
 Univ. of Houston  
 Houston, TX  
 ipavlidis@uh.edu

**Abstract**—Waveforms extracted via nasal thermistors are the most common signals used to study breathing function in sleep studies. In recent years, unobtrusive alternatives have been developed based on thermal imaging. Initially, the research aimed to produce a measurement on par with the clinical standard (the thermistor), but at a distance. Lately, there has been recognition that imaging is inherently multidimensional and can produce spatiotemporal and not just temporal signals - a development with significant diagnostic value. The extraction of 3D breathing information, however, has been based on inaccurate assumptions regarding the formation of the nasal thermal patterns sensed by the camera. The present paper corrects these assumptions, enabling the production of more accurate and complete multidimensional breathing signals.

**Keywords**-biomedical imaging; thermal imaging; 3D breathing information; breathing signal

### I. INTRODUCTION

The need for unobtrusive breathing monitoring in sleep studies is well documented. Multiple methods based on thermal imaging have been introduced in recent years. Murthy *et al.* captured the temporal evolution of the breathing function by averaging the thermal footprint of the exhaled/inhaled air around the nostrils; the method could operate only on a profile view of the nose [1]. Fei *et.al* performed the measurement on the nostrils themselves and not their vicinity, obtaining more robust results and at any viewing angle [2]. Fei's method, known as 'virtual thermistor', has on par capability and performance with clinical nasal thermistors, with the advantage of being non-contact (Fig. 1). The major criticism for the method is the loss of spatial information, which is inherently present in an imaging modality [3]. At every time step, Fei's method collapses the 2D thermal data from the nostrils into a mean value, thus, shedding away the spatial information.

Duong *et al.* introduced a thermal imaging method that preserves the temporal and spatial information of the breathing function [3]. The method attempts to delineate the spatial evolution of the breathing function in every thermal frame, stacking up the results along the time axis. The delineation is carried out through a level-set algorithm, which breaks down during exhalation. Hence, although inhalation information is well represented, the exhalation phase is denoted by a gap (no information). Duong reports a patient case with subtle

pathology, localized in a small area of one nostril, which is captured by his method while it is missed by the virtual thermistor method, due to its averaging nature. The example clearly illustrates the clinical potential of spatiotemporal breathing information.

The major problem with Duong's method is the assumption that the observed spatiotemporal evolution takes place on a plane that cuts through the tip of the nose. Implicit to this assumption is the notion that the thermal camera maps the emission of the inhaled or exhaled air as it passes through the nostrils. This is not true. In fact, what the thermal camera observes through the nostrils is the thermal emission from the inner nasal lining, extending back to the rhinion. The air's emittance contribution is close to negligible [4]. What the forced inhaled and exhaled air does, however, is to modulate the tissue emission according to heat convection laws [4]. Indeed, human tissue is a good thermal conductor [5] and an ideal thermal radiator (emissivity,  $e = 0.97$ ) [4], responding well to nasal air flow modulation and emitting a strong signal toward the thermal imaging sensor. (Fig. 1)

In this paper, we correct previously held assumptions about the formation of the nasal thermal pattern sensed by a thermal camera. The new model, described in the Methodology section, enables the construction of a stereoscopic view of the breathing function. Specifically, we use the parametric equation of an ellipsoid to model the geometric shape of the nostril's inner surface. At every time step, the ellipsoid surface is rendered with the modulated thermal map sensed by the camera. Key in this process is finding the correspondence between the pixel map and the ellipsoid map or in other words, mapping breathing functionality to the corresponding anatomical locations. We test the proposed method vs. the legacy method [3] on a pilot dataset, reporting results in the Experiments section. We conclude the paper with a brief discussion.

### II. METHODOLOGY

The nostril is a hollow structure. Farkas *et al.* [6][7] report seven nostril shapes which can be broadly classified into two groups: circular-shape and elliptical-shape (Fig. 2). Hence, we model the nostril anatomy via the parametric equation

# Subject 1

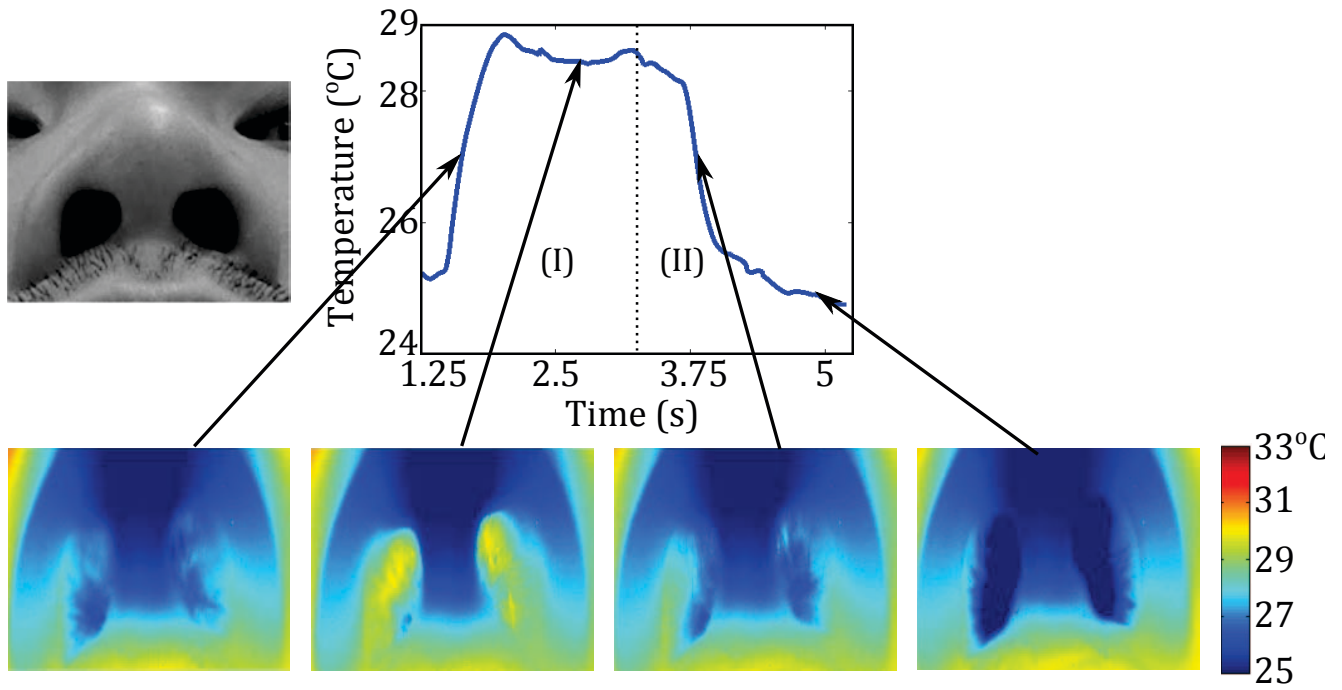


Figure 1. Virtual thermistor signal and thermal snapshots of the nostrils during a normal breathing cycle for Subject 1.

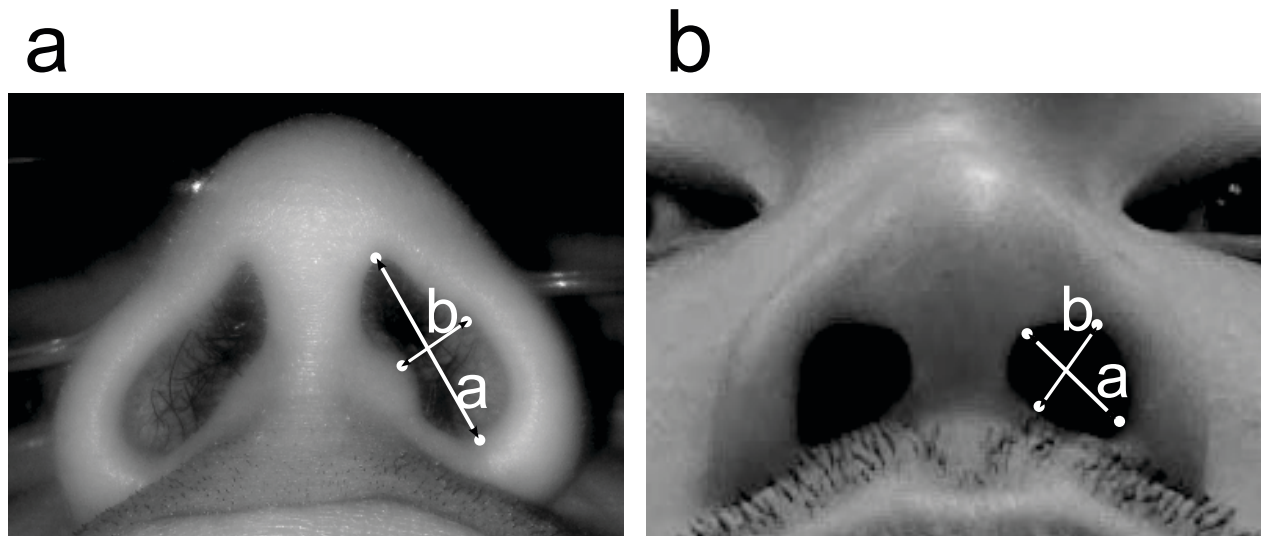


Figure 2. Nostril types: (a) elliptical-shape and (b) circular-shape.

of an ellipsoid. Next, we map the thermal signature of the breath onto the ellipsoid surface at every time step.

### A. Geometric Modeling

The surface of a semi-ellipsoid is parameterized as follows:

$$\begin{aligned} x &= \frac{a}{2} \sin \phi \cos \theta \\ y &= \frac{b}{2} \sin \phi \sin \theta \\ z &= c \cos \theta \end{aligned} \quad (1)$$

where,  $\phi \in [0, 2\pi)$  and  $\theta \in [0, \pi/2]$ . The parameters  $a$  and  $b$  represent the longitudinal and transverse dimensions of the nostril openings, measurable with a Vernier caliper. The parameter  $c$  represents the depth of the nasal airway. Specifically, for every point  $i$  on the interior nasal surface,  $c_i$  represents its distance from the nostril's deepest point.

The measurement of the parameter  $c$  is more difficult than the parameters  $a$  and  $b$ . Also, to the best of our knowledge, there is no measurement technology to generate a distance map of the nasal cavity's interior surface. For this reason, we developed an image processing approach to approximate the parameter  $c$ . We use the Fast Marching method, which computes the time  $T$  at which a contour crosses a point  $(x, y)$  [8]:

$$|\nabla T(x, y)| V(x, y) = 1; \quad (x, y) \in \Omega \quad (2)$$

where,  $\Omega \in \mathbf{R}^2$  is an open set with a well-behaved boundary, and  $V(x, y)$  is a speed function. Once the arrival time  $T(x, y)$  is known, the travel distance  $c(x, y)$  can be computed. For simplicity, we assume that airflow in the nasal pathway is laminar ( $V(x, y) = \text{constant}$ ). Thus, the distance  $c(x, y)$  is proportional to the arrival time  $T(x, y)$ .

The method is initialized by positioning the ellipsoid, so that its tip is co-located with the deepest viewable point of the nasal canal (close to the rhinion). Due to the canal's stenosis, this is the area that is expected to exhibit maximum temperature change during a breathing cycle. Therefore, the method marks on the nostril's planar thermal map (sensed by the camera) the area that exhibits maximum variance during a breathing cycle; it uses this as the initialization position (Fig. 3). At the initial position  $(x_0, y_0)$ ,  $T(x_0, y_0) = 0$  and therefore, the distance  $c(x_0, y_0) = 0$ . In the next step, the method computes the distance map for the pixels that are closest to the initial position. Next, the method computes the distance map for the next nearest neighboring pixels, and so on. Thus, iteratively, it computes the distance for every pixel, enabling the stereoscopic mapping of the planar thermal map.

Please note that the interior nasal surface viewed by the thermal camera is only part of the overall nasal surface (alar). The method computes the distance map for the exposed area only. The parameters  $a$ ,  $b$  and  $c$  are normalized to the range  $[0, 1]$ , in order to facilitate inter-subject analysis.

Fig. 3 illustrates the ellipsoid construction of a nostril and its 'viewable' thermal signature, as it is sensed by the camera's focal plane array. At every time step, we render the surface texture of this ellipsoid by mapping the thermal signature onto it (via the distance map).

## III. EXPERIMENTS

### A. Experimental Design

We recorded with a Mid-Wave Infra-Red (MWIR) FLIR SC6000 camera [9] the evolving thermal signature of the nostrils from  $n = 6$  subjects. The thermal camera was placed approximately 2 ft away from each subject and each recording lasted about 100 s. The camera was outfitted with a 100 mm lens and a ring extender, to maximize focal length and enhance the spatial detail. The spatial resolution of the camera is  $620 \times 480$  pixels and its temporal resolution is 80 frames per second. The time duration of each recording was sufficient to capture multiple breathing cycles. Subjects S1, S2, S3 and S5 had normal breathing cycles, while Subjects S4 and S6 had a small polyp in one of their nostrils. The experiment was carried out according to an institutionally approved protocol.

### B. Experimental Results

In the main body of Fig. 4, each row illustrates the evolving 3D reconstruction of a normal breathing cycle on the left nostril of Subject S1, S2, S3, and S5, respectively. The bottom of each 3D panel represents the subject's nostril, while its top represents the subject's rhinion level. The rendered surface corresponds to the viewable nasal interior.

The surface texture indicates that the heat convects non-uniformly from the nostril to the nasal canal's deeper areas. In the beginning of the exhalation period, the deeper area is relatively cooler than the area closer to the nostril. As the subject exhales hot air (phase/column **a** in Fig. 4), the nasal lining absorbs the heat. The heat convects at a faster rate to a cool surface than to a warm surface [10]. Hence, the deepest area absorbs more heat than the area closer to the nostril. At the exhalation peak (phase/column **b** in Fig. 4), the nasal lining nearly equilibrates at all depths, becoming more uniform.

As the subject inhales cool atmospheric air, the nostril's lining loses heat due to abduction. Hence, the uniform texture at the beginning of the inhalation period increasingly becomes non-uniform toward the end of the period (phase/column **c** in Fig. 4). In particular, the deepest area loses heat at much faster rate than the area closer to the nostril. This is thanks to the higher speed the inhaled air attains in the deepest point, due to the nasal canal's stenosis at the rhinion.

The top of Fig. 4 shows the temporal breathing signal computed according to the method reported in [2] and column **d** in Fig. 4 shows the spatiotemporal breathing reconstruction for Subject S1, S2, S3, and S5, according to the

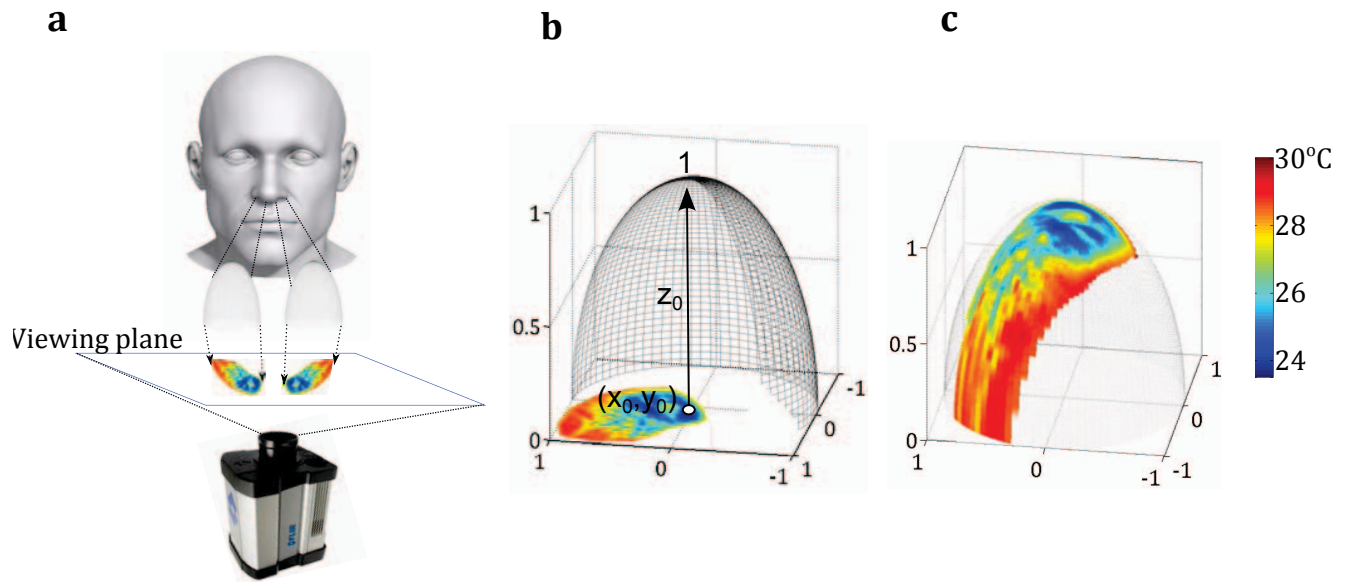


Figure 3. **a**, Experimental layout. **b**, Ellipsoid modeling of the nasal airway and its arrangement with respect to the thermal image of the left nostril. **c**, Mapping of the thermal image to the ellipsoid surface viewable through the nose’s alar.

legacy method reported in [3]. That spatiotemporal method captures mainly the inhalation phase, while it provides no information during the exhalation phase. The method treats the thermal map as planar and attempts to capture curve evolution via level sets, which they break when the map nearly saturates during exhalation. By contrast, our method treats the thermal map as a 3D projection and performs the depth mapping, via a model based on anatomical constraints (rhinion) and functional physics (heat transfer).

Fig. 5 illustrates the 3D reconstruction of breathing for both nostrils of Subject S4 and S6 - the right nostrils in both subjects have small polyps, locally stemming the effect of air flow. The thermal map never really saturates at the rhinion of the pathological nostrils. This is missed in the virtual thermistor signal (Fig. 5). However, it is evident in the spatiotemporal signal (Fig. 5d) as a ‘bridge’, during a period (i.e., exhalation) in which one would expect to see nothing produced by this method. The 3D projection on the ellipsoid in Fig. 5, clearly provides the most complete information, which includes not only the presence of the localized abnormality, but also all the other functional detail and in its correct anatomical position.

### C. Discussion

The 3D method of breathing reconstruction put forward in this paper, rights the deficiencies of earlier spatiotemporal reconstruction methods [3] in thermal imaging. Evolution of anatomically mapped breathing signals (during both inhalation and exhalation) are now feasible, broadening

the diagnostic value of unobtrusive measurement methods beyond sleep studies to ENT and pulmonary medicine. The pilot experiments demonstrate that the method can detect small obstructive abnormalities, such as nasal polyps, which locally stem airflow, leaving a persistent print on the ellipsoid map.

For short imaging sessions, such as the pulmonary tests performed in our experiments, the subject can be asked to remain still and a tracker is not necessary. However, for long sessions (such as a full nocturnal sleep study), a tracker similar to the one reported in [11] would be needed.

### REFERENCES

- [1] R. Murthy, I. Pavlidis, and P. Tsiamyrtzis, “Touchless monitoring of breathing function,” in *Proceedings of the 26th Annual International Conference of the IEEE Engineering in Medicine and Biology Society*. IEEE, 2004, pp. 1196–1199. 1
- [2] J. Fei and I. Pavlidis, “Thermistor at a distance: Unobtrusive measurement of breathing,” *IEEE Transactions on Biomedical Engineering*, vol. 57, no. 4, pp. 988–998, 2010. 1, 3, 5, 6
- [3] D. Duong, D. Shastri, P. Tsiamyrtzis, and I. Pavlidis, “Spatiotemporal reconstruction of the breathing function,” in *International Conference on Medical Image Computing and Computer-Assisted Intervention*. Springer, 2012, pp. 149–156. 1, 4, 5, 6
- [4] D. Pitts and L. Sissom, *Heat Transfer*. McGraw Hill, 1997. 1

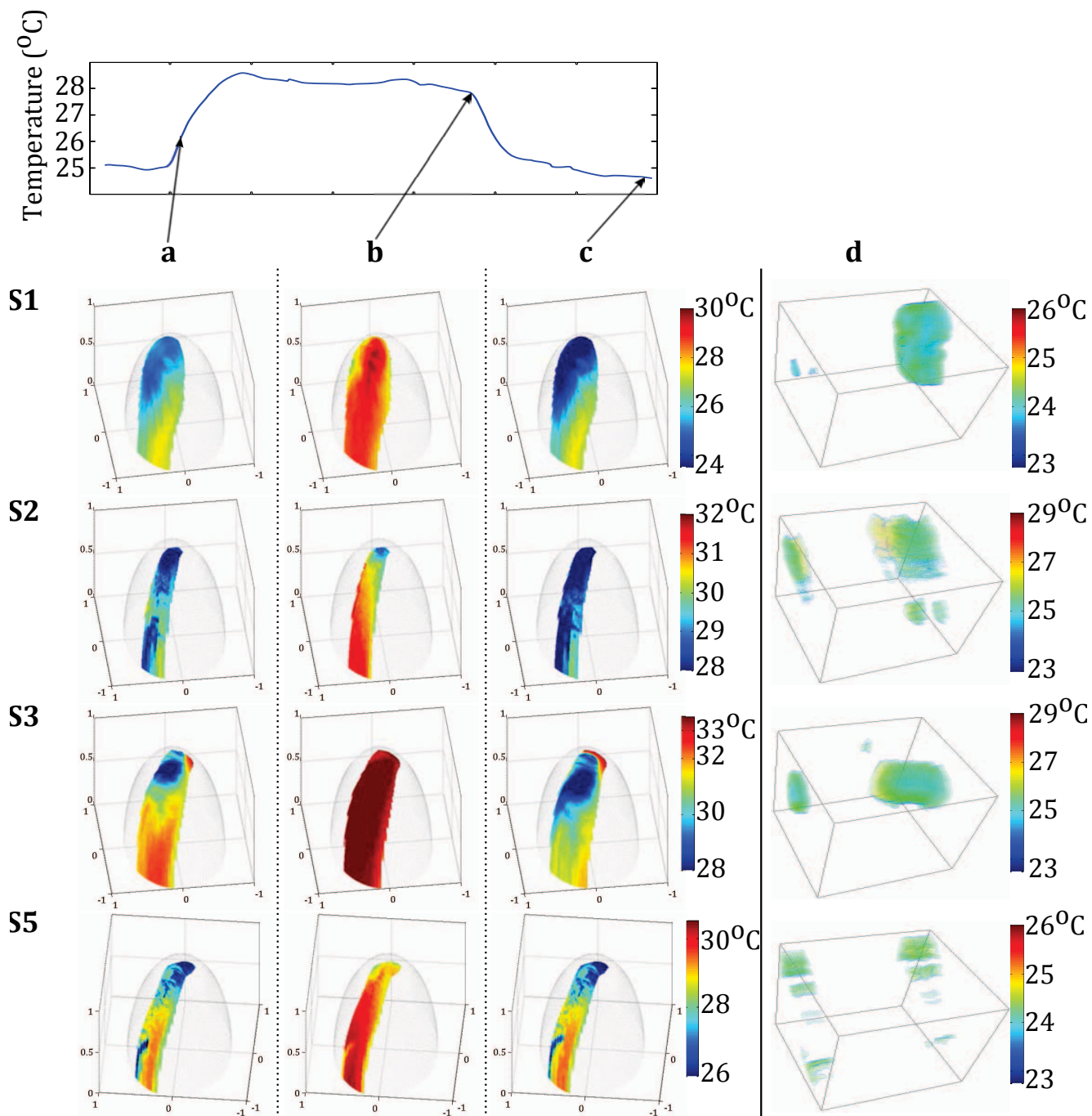


Figure 4. Normal breathing cycles on the left nostrils of four subjects (S1, S2, S3, S5). TOP: Temporal reconstruction according to the virtual thermistor method reported in [2] for subject S1. Mapping on the ellipsoid model per subject: **a**, in mid-exhalation; **b**, at the end of exhalation; **c**, at the end of inhalation. **d**, Spatiotemporal reconstruction according to the method reported in [3] for comparison.

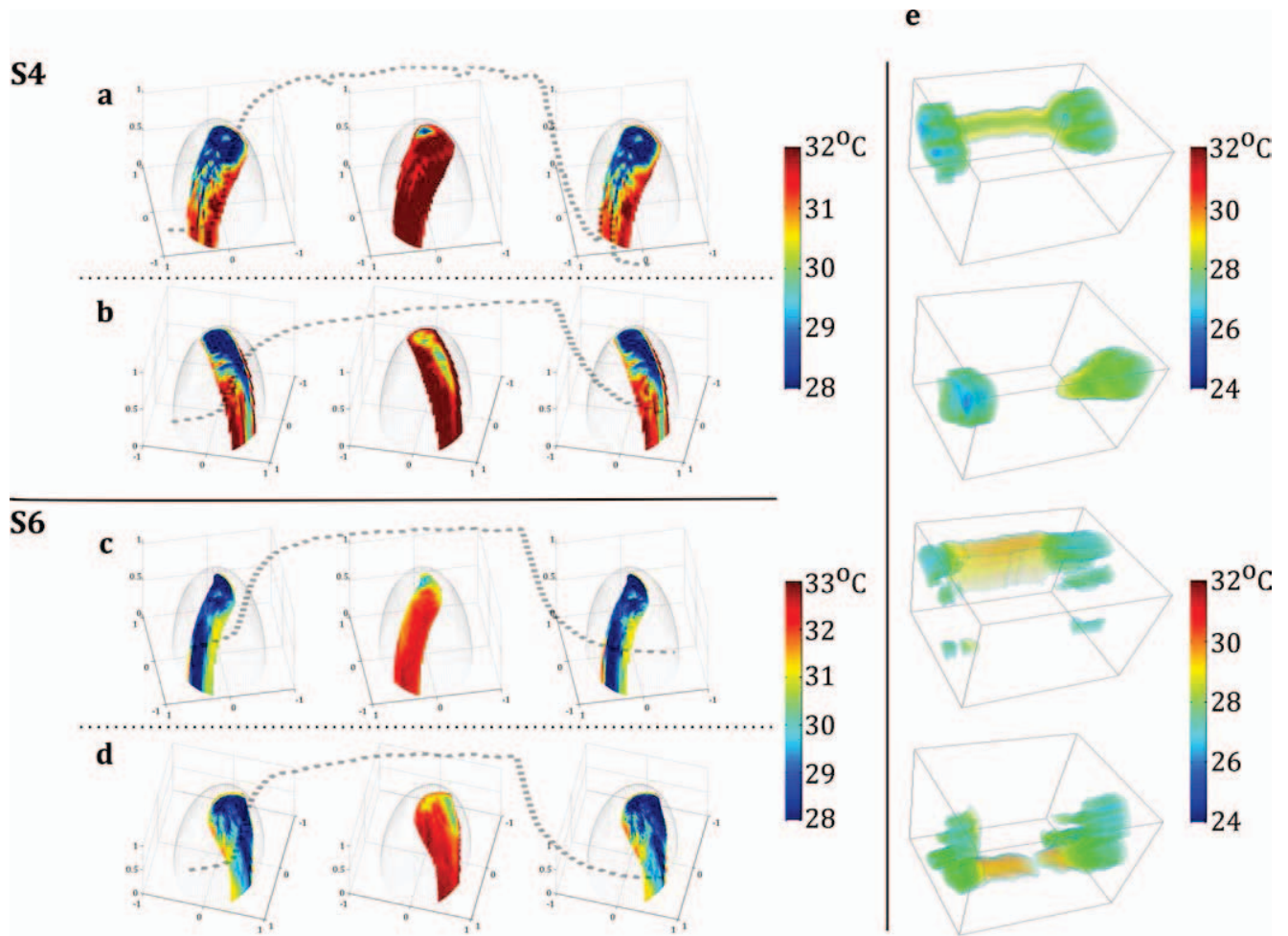


Figure 5. Normal and pathological breathing cycles in subjects S4 and S6. In dotted lines appear the virtual thermistor signals computed according to [2]. **a**, S4's right nostril with nasal polyp, stemming flow (persistent spot at the top). **b**, S4's left nostril. **c**, S6's right nostril with nasal polyp, stemming flow (persistent spot at the top). **d**, S6's left nostril. **e**, Corresponding spatiotemporal models according to [3] for comparison.

- [5] M. Cohen, "Measurement of the thermal properties of human skin. A review," *Journal of Investigative Dermatology*, vol. 69, pp. 333–338, 1977. 1
- [6] L. Farkas, T. Hreczko, and C. Deutsch, "Objective assessment of standard nostril types: A morphometric study," *Annals of Plastic Surgery*, vol. 11, no. 5, pp. 381–389, 1983. 1
- [7] L. Farkas, J. Kolar, and I. Munro, "Geography of the nose: A morphometric study," *Aesthetic Plastic Surgery*, vol. 10, no. 1, pp. 191–223, 1986. 1
- [8] J. A. Sethian, "A fast marching level set method for monotonically advancing fronts," *Proceedings of the National Academy of Sciences*, vol. 93, no. 4, pp. 1591–1595, 1996. 3
- [9] FLIR, <http://www.flir.com>. 3
- [10] W. McAdams, *Heat Transmission*. McGraw Hill, 1954. 3
- [11] Y. Zhou, P. Tsiamyrtzis, P. Lindner, I. Timofeyev, and I. Pavlidis, "Spatio-temporal smoothing as a basis for facial tissue tracking in thermal imaging," *IEEE Transactions on Biomedical Engineering*, vol. 60, no. 5, pp. 1280–1289, 2013. 4